Developmental Self-Assembly of a DNA Tetrahedron

John P. Sadowski,[†,‡] Colby R. Calvert,[⊥] David Yu Zhang,[†,§] Niles A. Pierce,[⊥,∥] and Peng Yin[†,§,*]

[†]Wyss Institute for Biologically Inspired Engineering, Harvard University, Boston, Massachusetts 02115, United States, [‡]Department of Chemistry and Chemical Biology, Harvard University, Cambridge, Massachusetts 02138, United States, [§]Department of Systems Biology, Harvard Medical School, Boston, Massachusetts 02115, United States, [⊥]Division of Biology and Biological Engineering, California Institute of Technology, Pasadena, California 91125, United States, and [∥]Division of Engineering and Applied Science, California Institute of Technology, Pasadena, California 91125, United States

ABSTRACT Kinetically controlled isothermal growth is fundamental to biological development, yet it remains challenging to rationally design molecular systems that self-assemble isothermally into complex geometries *via* prescribed assembly and disassembly pathways. By exploiting the programmable chemistry of base pairing, sophisticated spatial and temporal control have been demonstrated in DNA self-assembly, but largely as separate pursuits. By integrating temporal with spatial control, here we demonstrate the "developmental" self-assembly of a DNA tetrahedron, where a prescriptive molecular program orchestrates the kinetic pathways by which DNA molecules isothermally self-assemble into a well-defined three-dimensional wireframe geometry. In this reaction, nine DNA reactants initially coexist metastably, but upon catalysis by a DNA initiator molecule, navigate 24 individually characterizable intermediate states *via* prescribed assembly pathways, organized both in series and in parallel, to arrive at the tetrahedral final product. In contrast to previous work on dynamic DNA nanotechnology, this developmental program coordinates growth of ringed substructures into a three-dimensional wireframe superstructure, taking a step toward the goal of kinetically controlled isothermal growth of complex three-dimensional geometries.

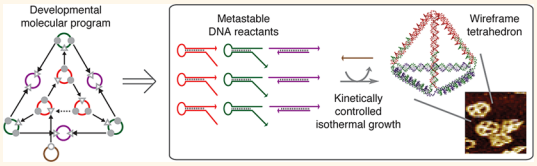

KEYWORDS: molecular programming · DNA nanotechnology · kinetic pathway control · developmental self-assembly

Molecular self-assembly, a fundamental process underlying the development and operation of biological organisms, has emerged as an important engineering paradigm for nanotechnology. Biological development controls molecular arrangement both spatially and temporally to produce a complex organism that robustly responds to its chemical and physical environment. By contrast, it has remained challenging to achieve sophisticated spatial and temporal control in an integrated fashion in rationally designed synthetic biomolecular systems.

There have been many recent advances in the design of sophisticated synthetic nucleic acid systems that enable either spatial or temporal control of molecular self-assembly, but these two capabilities have largely been relegated to separate realms. Past work in structural DNA nanotechnology,[1−3] including the synthesis of ribbons,[4,5] tubes,[5,6] two- and three-dimensional extended crystals,[6−11] and discrete objects,[12−21] has largely had the goal of engineering static target structures, without an explicit focus on controlling the assembly order and transient dynamics of how individual units come together to produce such a target structure. Conversely, past work in dynamic DNA nanotechnology,[22,23] including demonstrations of reconfigurable devices,[24,25] autonomous logical circuits,[26−29] dynamic self-assembling systems,[28,30,31] and walkers,[28,32−35] has typically focused on either engineering the transient interaction pattern of the individual molecular species to achieve desired computational or kinetic behavior, without explicit concern for the structural properties that the assembling and disassembling molecular species produce, or has introduced limited reconfigurability to an otherwise static structure.

To capture the complexity and robustness of molecular self-assembly demonstrated by the biological developmental process, it is necessary to design the temporal in addition to the spatial order of self-assembly. This would allow direct, molecular-scale kinetic control over the entire assembly pathway, rather than being limited to specification of the final structure only.

* Address correspondence to py@hms.harvard.edu.

Received for review July 23, 2013 and accepted February 19, 2014.

Published online April 11, 2014
10.1021/nn4038223

Such a system would no longer need a thermal annealing step to initiate the assembly and encourage the dominance of the desired, lowest-energy product; the reaction could instead proceed isothermally and *in situ* with a molecular input to trigger the assembly. This would allow the construction of a "developmental" self-assembly system where a synthetic structure "grows" following prescribed kinetic assembly pathways organized both in series and in parallel, with some reactions occurring sequentially and others occurring simultaneously, ultimately developing into the desired complex target structure.

To address this largely unexplored challenge of integrating temporal control with spatial control in synthetic molecular self-assembly, we demonstrate here the rational design and kinetically controlled isothermal synthesis of a DNA tetrahedron with a well-defined three-dimensional wireframe structure. The assembly is the execution of a developmental molecular program specified using a reaction graph abstraction[28] that describes the kinetic pathways by which the DNA reactants self-assemble and disassemble. This work builds on a previous demonstration of programming molecular self-assembly and disassembly pathways using a versatile DNA hairpin motif, to execute diverse molecular programs including catalytic formation of branched junctions, cross-catalytic circuitry, conditional assembly of dendritic structures, and autonomous locomotion.[28] Unlike these previous demonstrations, the current molecular program yields a well-defined three-dimensional wireframe structure formed from closed rings. In contrast to DNA origami and tile-based approaches to structural DNA nanotechnology, our method is initiated by a catalytic molecular trigger, works isothermally within a wide temperature range, and follows a predetermined kinetic pathway. We envision that our strategy for rationally designing developmental molecular programs can be generalized to more complex three-dimensional wireframe constructions.

RESULTS AND DISCUSSION

Kinetic Pathway Design. The tetrahedron assembles from six hairpins,[28] divided into **A** and **B** groups, and three cooperative hybridization complexes[37] making up the **C** group (Figure 1a). The hairpins are designed with structures that initially keep key sequence domains, called toeholds,[24] inaccessible; each hairpin can then be opened by a specific initiator strand, allowing the newly accessible toeholds to participate in downstream reactions. Cooperative hybridization complexes each bind to two initiators and are used in ring formation reactions. Thus, the reactants as a group are metastable, so that no reaction appreciably proceeds in the absence of the initiator, but in the presence of the initiator the assembly reaction happens autonomously and follows prescribed kinetic assembly pathways without the need for external intervention. The final product is a three-dimensional tetrahedron with edges 18 nm long, each containing five turns of DNA (Figure 1b).

The assembly of the tetrahedron represents the execution of a prescribed molecular program. The program is depicted as a reaction graph using a nodal abstraction that concisely describes the kinetic pathways by which DNA reactants self-assemble and disassemble.[28] The reaction graph emphasizes the functional relationship between reactant complexes rather than the detailed structures of each reactant (Figure 1c). Each molecular species is represented by a node depicted as a black ring containing triangles representing input ports, and circles representing output ports. The initial state of a port is either 'accessible' (open symbol) or 'inaccessible' (solid symbol). The ports are functionally connected through an internal logic that toggles their states during the execution of the program, as described below. A developmental molecular program is written as a reaction graph by connecting complementary output and input ports on different nodes *via* either assembly operations (solid arrow) or disassembly operations (dashed arrow).

The reaction graph precisely defines which reactions must occur in series and which reactions may occur in parallel. For the tetrahedron, the reaction can only start with the assembly of **I** to **A1**, because this is the only assembly reaction where both participating ports (the output port on **I** and the input port on **A1**) are initially accessible. The **B1** and **A2** nodes cannot assemble with **A1** until **A1** has been opened (*via* assembly with **I**) and its output ports have become accessible, but these two assembly reactions are not dependent on each other because they are on separate branches downstream of the **A1** assembly. This is in contrast with traditional thermodynamic assemblies, where all parts of each molecule are initially accessible, with no explicit control of assembly order (Figure 1c, right).

The ports each correspond to a physical region on a strand or complex that has a single function during the assembly process. For hairpins, the single input region is represented by an orange triangle, and the two output regions are colored according to their position: the blue ports overlap the loops, while the green ports overlap the tails. The nodal abstraction is capable of representing the state of the molecular program at various points in its execution: in a hairpin assembly reaction (Figure 1d, top), the hairpin input port and the corresponding initiator output port are both initially open, indicating that a reaction is possible. After assembly, a line is drawn between these ports indicating that they are now bound, and, importantly, the two output ports on the hairpin change state from closed to open. This corresponds to the structural change, where the 1* toehold on the single-stranded initiator

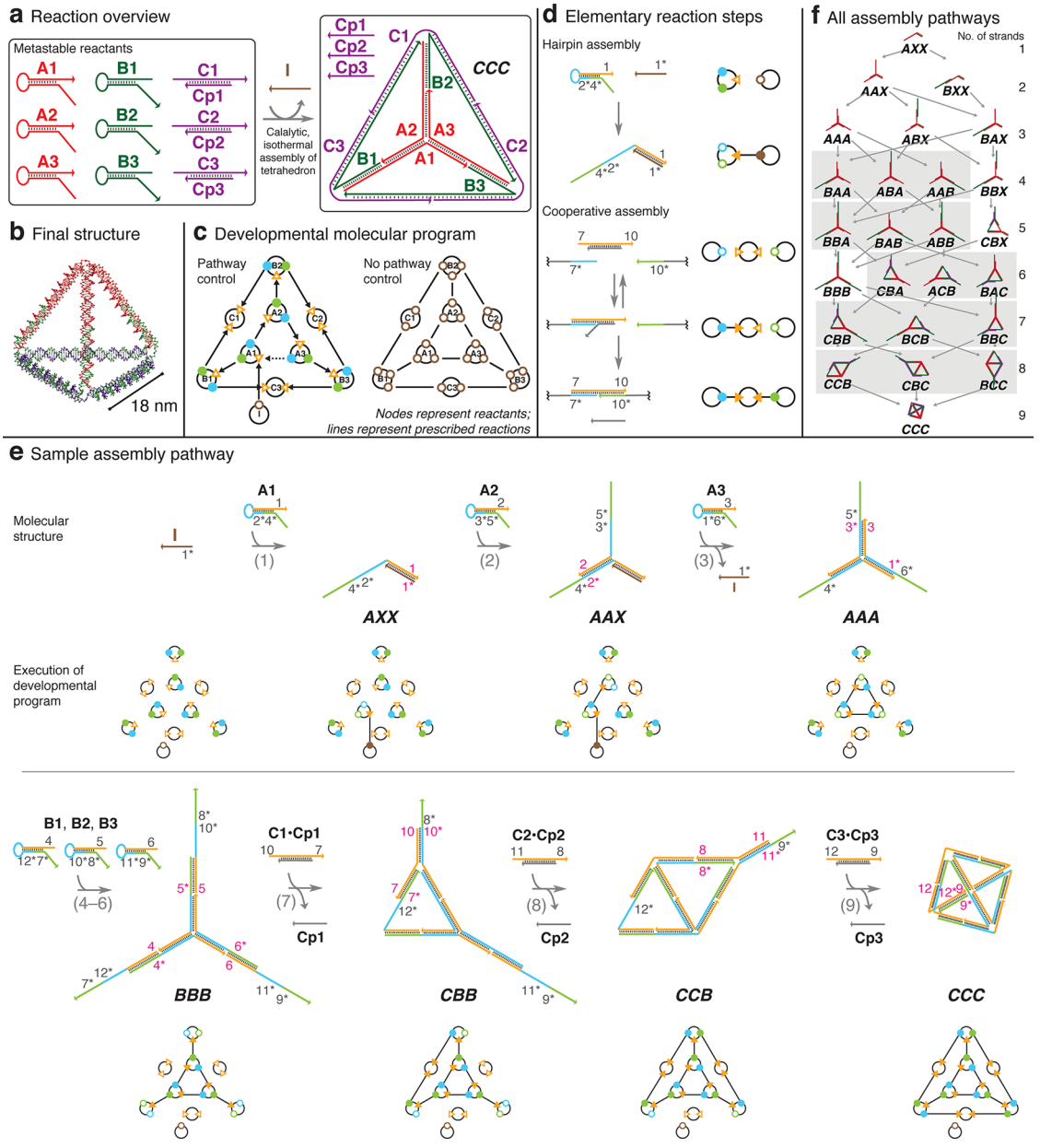

Figure 1. Catalytic self-assembly of a DNA tetrahedron. (a) Overview of the reaction. (b) A computer-rendered model[36] of the tertiary structure of the assembled tetrahedron. (c) The reaction graph of the developmental molecular program specifying kinetically controlled self-assembly (left) compared to a traditional self-assembly process that lacks pathway control (right). Solid and dashed arrows depict kinetically controlled assembly and disassembly operations; line segments depict assembly operations that are not kinetically controlled. (d) Execution schematics of two elementary reactions. Left, molecular structures; right, corresponding nodal abstractions, where lines are added to connect ports once assembly has occurred. The strand regions are colored the same as the corresponding ports in the nodal representation. Top, a hairpin assembly reaction. Bottom, a cooperative assembly reaction. (e) Execution of the developmental molecular program along one possible assembly pathway. Only active toehold domains are labeled in this figure, with newly hybridized toeholds labeled in pink. Top, molecular structures; bottom, corresponding nodal execution schematics. See Supporting Information Figure S1 for a schematic showing all sequence domains. (f) The full set of intermediates along the prescribed assembly pathways. A three-letter code is used to identify each species as explained in the text. Species that are structurally congruent are linked by gray boxes. The numbers of assembled strands (excluding the initiator) for each row are displayed. The pathway in panel e corresponds to the reactions along the left edge of this figure.

hybridizes with the exposed 1 toehold on the hairpin, beginning a strand displacement that opens the hairpin and exposes the two initially hidden toeholds 2* and 4*. A disassembly reaction[28] (not shown) is represented by a dashed arrow, and represents the displacement of a previously assembled port with a new one. This type of reaction is used in the tetrahedron to displace the initiator partway through the assembly, allowing it to catalyze the assembly of further tetrahedra.

Cooperative complexes,[37] rather than hairpins, were used for the ring forming reactions because they were observed to reduce the formation of aggregates

and multimeric products, which are the result of intermolecular interactions outcompeting the desired intramolecular ones (see Supporting Information Section S3.3). Cooperative hybridization complexes contain two toeholds and are assembled into the growing complex only in the presence of both initiator domains (Figure 1d, bottom). This is because the singly bound intermediate is short-lived due to the fact that neither initiator domain can fully displace the protector strand by itself, leading to quick disassembly if the second initiator is not immediately available.[37] In molecular terms, the depicted cooperative complex has two toeholds, 7 and 10. Upon binding to the exposed 7* toehold in the blue initiator, the protector strand is partially displaced. This initial reaction is by itself reversible; in the absence of the green initiator, the blue initiator will rapidly disassemble. However, if the green initiator with toehold 10 is also present, the 10 and 10* toeholds may then bind, allowing the protector strand to be completely and irreversibly displaced. In the tetrahedron, all cooperative assembly events are intended to occur intramolecularly, involving two initiator domains on the same molecule, and thus, each such assembly causes the formation of a ring. See Supporting Information Section S4 for additional details on the nodal abstraction and reaction graphs.

Figure 1e depicts an example execution trajectory for the molecular program. The top panel shows the molecular structures and the bottom panel shows the corresponding state of the molecular program using the nodal abstraction. The assembly begins with the sequential opening of the **A1**, **A2**, and **A3** hairpins causing self-assembly of a three-arm junction[28] corresponding to the first vertex of the tetrahedron (reactions 1−3). The initiator **I** is released upon completion of the junction (reaction 3), allowing it to catalyze the assembly of further tetrahedra. Next, each arm of this junction then extends to incorporate the **B1**, **B2**, and **B3** reactants through another set of hairpin opening reactions (reactions 4−6). Finally, the overhanging portions of the **B** strands are involved in three ring forming reactions using a set of cooperative hybridization complexes[37] incorporating the **C1**, **C2**, and **C3** strands (reactions 7−9).

Because the assembly was designed to proceed in a branched fashion, the assembly of the three independent branches is not synchronized. Thus, there are multiple potential paths leading to the desired product, involving a total of 24 on-pathway intermediates (Figure 1f). We identify each intermediate of the tetrahedron formation with a three-letter code where each letter denotes the progress of one of the three branches of assembly. For example, in the intermediate ***ABA***, **A1** has been incorporated in the first branch, **A2** and **B2** are in the second branch, and **A3** is in the third branch (note again that **A2** incorporation is a prerequisite of **B2** incorporation). Letter ***X*** is used to denote the lack of assembly of the **A** strand along the corresponding branch; if the third letter is ***X***, the initiator **I** is still attached (for example, ***AAX*** contains **A1**, **A2**, and **I**). See Supporting Information Figure S3 for a detailed description of the codes. Note that complexes that are related by cyclic permutations of their abbreviations have congruent secondary structures; these are linked by gray boxes in the figure.

Gel Electrophoresis Studies. We studied the formation of the tetrahedron using a gel electrophoresis mobility shift assay (Figure 2), where each intermediate was individually synthesized by mixing the initiator with different subsets of the nine reactants of the tetrahedron assembly. We were able to observe the formation of each of the 24 possible intermediates as a distinct band in a native polyacrylamide gel (lanes 2−25). Intermediates with greater numbers of incorporated strands migrated more slowly, with the exception of the ring formation transitions, which tended to have unpredictable effects (*e.g.*, ***BBX*** → ***CBX*** and ***BBA*** → ***CBA*** showed little mobility change, and ***BBB*** → ***CBB*** showed increased mobility). This is likely because the first ring formation reduces the angle between two of the arms from its natural angle to ≈60°, making the complex more compact. Groups of intermediates with congruent structures, linked by the gray boxes in the figure, were observed to have nearly identical mobility, consistent with our expectations. The band identified as the assembled tetrahedron (lane 26) had a mobility distinct from any of the intermediates. The lower-mobility bands above the tetrahedron band are hypothesized to be multimers of the tetrahedron structure, formed when assembly of the cooperative complexes cause the intermolecular joining of two different growing tetrahedra rather than the desired intramolecular ring forming reactions (Supporting Information Figure S4).

When all reactants except **I** were incubated together (lane 30), only a small amount of unintended "leakage" products was observed: 3.5% of the signal was in the product band and 80% was in the reactants band. When at least 0.25 equiv of **I** was included (lanes 26−28), the reaction proceeded to completion (that is, all **A1** hairpins were consumed), indicating a catalytic turnover of at least 4. Typical yields of the tetrahedron varied between 20 and 40%, depending on concentration (Supporting Information Figure S5). At a higher reactant concentration (100 nM, lanes 1−30), the dominant side products were the higher-weight products, while at a lower concentration (10 nM, lanes 31−35), the dominant side products were intermediates of lower molecular weight. Varying the toehold lengths of the cooperative complexes was not observed to qualitatively improve the reaction yield (Supporting Information Figure S6).

We observed that the reaction yield was primarily bottlenecked by the ring-forming reactions. On the

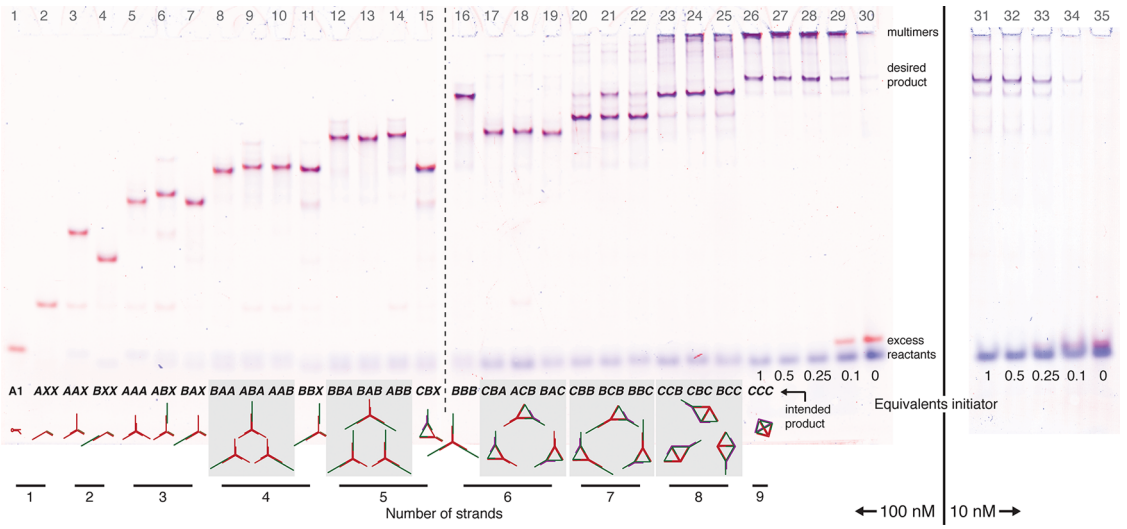

Figure 2. Characterization of the tetrahedron assembly pathway. This is a gel electrophoresis mobility shift assay where lanes 1−25 show all on-pathway intermediates of the tetrahedron assembly, formed by mixing different subsets of reactants with the initiator. Gray boxes mark groups of intermediates that are structurally congruent and expected to have the same mobility, and the structures of the intended products are shown, as in Figure 1f. Lanes 26−35 show the analysis of catalytic turnover at two concentrations, showing reactions containing all nine reactants but varying concentrations of initiator I. These are 6% native polyacrylamide gels of assembly reactions containing 1 equiv of all reactants at the specified concentration, except A1 for which we used 0.9 equiv of a FAM fluorophore-labeled hairpin to observe incorporation yields. The initiator was included at 1 equiv unless otherwise specified in the figure. The assembly reactions were conducted at room temperature in TAE/Mg^{2+} buffer containing 12.5 mM Mg^{2+} over 19 h. The dotted line separates two gel slabs that were run simultaneously, and the solid line separates gels that were run at different times. The intensity of the FAM fluorescent label is shown in red, and SYBR Gold staining intensity is shown in blue; these channels are separated in Supporting Information Figure S2. See Supporting Information Figure S4 for an agarose gel of these same samples, in which the side products of higher molecular weight are well-resolved.

basis of analysis of Figure 2, the yield of ***BBB***, the largest intermediate with no rings, was 83% for six hairpin incorporation events. However, the average yield of the seven intermediates containing one **C** strand, and thus one formed ring, dropped to 71%. With two **C** strands, the yield was reduced to 50%, and the yield of the full tetrahedron was only 19%. This drop in yield is likely the result of undesired intermolecular interactions outcompeting the desired intramolecular ring formation during the assembly of the cooperative complexes. This may be exacerbated by steric strain introduced in the ring formations. Although the single-nucleotide spacers and nicks at each junction were meant to relieve this strain, it is not clear if this was sufficient, and the use of longer single-stranded spacers at the vertices might further improve the yield.

Gel electrophoresis studies showed that the assembly is temperature-robust, working isothermally at temperatures in roughly the range 16−41 °C (Supporting Information Figure S7). At room temperature at 100 nM, the assembly reaction was observed to be complete after 9 h (Supporting Information Figure S8).

While the unique mobility of the ***CCC*** band indicates that all nine strands are incorporated into a single complex, additional assays are required to demonstrate ring formation and distinguish it from, for example, a large floppy three-arm junction. To demonstrate the ring formation, we conducted a fluorescence-quenching assay (Figure 3), using **C** strands functionalized with a fluorophore and optionally a quencher. The formation of each ring caused the fluorophore from one **C** molecule to become colocalized with the quencher on the neighboring strand, quenching the fluorescent signal. For example, lane 1 contained a ***CBB*** complex where a red fluorophore was attached to the **C1** strand; as expected, a red fluorescent band was visible on the gel. Lane 2 contained a ***CCB*** complex where red and green fluorophores were, respectively, attached to the **C1** and **C2** strands; both red and green fluorescence were detected in the target band, as expected. Lane 3 showed another ***CCB*** complex which additionally had a quencher attached to the **C2** strand; here, green but not red fluorescence signal was detected, indicating that proper ring formation had resulted in the colocalization of the quencher on **C2** with the red fluorophore on **C1**, thus removing the red fluorescence from the product band. In the full tetrahedron, all three fluorophores were fully visible in the absence of quenchers (lane 10) but fully quenched when quenchers were added (lane 11), indicating that all three ring formations were simultaneously successful, and that the tetrahedron's overall structure formed as designed.

Microscopy Studies. We further confirmed the correct formation of the geometric structures of the tetrahedron and its key intermediates using atomic force microscopy (AFM). ***BBB*** appeared as a three-arm

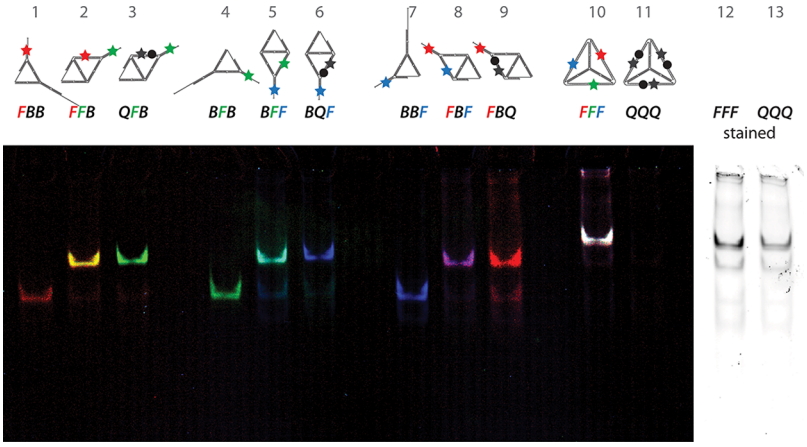

Figure 3. Characterization of ring-forming reactions. In this fluorescence-quenching assay, each of the three C strands was functionalized with a different fluorophore at its 5′ end (C1—TYE 665, red; C2—TAMRA, green; C3—FAM, blue); *F* represents a C strand with a fluorophore only, while *Q* represents a strand with a fluorophore expected to be quenched by a quencher on the 3′-end of a neighboring C strand. Lanes 1—3 show the structures *FBB* (*CBB* with a red fluorophore on the C1 strand), *FFB* (*CCB* with red and green fluorophores on the C1 and C2 strands, respectively), and *QFB* (*CCB* with the same two fluorophores, plus a 3′-quencher on the C2 strand that quenches the red 5′-fluorophore on the C1 strand). Lanes 4—6 and 7—9 show the other two structural permutations. Lane 10 shows *FFF* (the full tetrahedron with all fluorophores), and lane 11 shows *QQQ* (the full tetrahedron with all fluorophores and all quenchers). Lanes 12 and 13 are the same lanes in the same gel as lanes 10 and 11, but after staining with SYBR Gold. This is a 6% native polyacrylamide gel of a 10 nM assembly reaction with 1 equiv of initiator, conducted at room temperature in TAE/Mg^{2+} buffer containing 12.5 mM Mg^{2+} over 22 h.

junction, ***CBB*** as a single triangle, ***CCB*** as a double triangle, and ***CCC*** as a flattened tetrahedron, all consistent with their designed shapes (Figure 4a). Additionally, digestion at an intentionally engineered endonuclease restriction site on a specific edge converted a full tetrahedron back to a double triangle pattern under AFM, as expected. The double triangle structure contained two noncongruent types of vertices, which were distinguished by attaching a streptavidin molecule to one of them; digestion with either of two endonucleases targeted to two different edges yielded images of structures with the streptavidin on the expected vertex, further confirming the correct formation of the full tetrahedron (Figure 4b).

CONCLUSIONS

We have extended the pathway-controlled DNA self-assembly approach,[28] demonstrating the developmental growth of a well-defined three-dimensional wireframe DNA tetrahedron, formed from metastable reactants conditionally in the presence of a single-stranded trigger and through a kinetically programmed pathway. In particular, this is the first catalytic self-assembly design that incorporates ring forming events, a potentially useful topological primitive for the growth of larger assemblies with well-defined geometries. Ring formation is challenging because the desired intramolecular reaction that forms the ring must compete with off-pathway intermolecular reactions that lead to multimers and other aggregation side products. Using cooperative hybridization complexes for the ring forming reactions appears to avoid significant difficulties encountered with a set of noncooperative designs (Supporting Information Section S3.3). We believe that even greater improvements in yield could be achieved by designing the geometry of ring forming steps so that they do not require such large conformational changes in the molecule. This would favor the desired intramolecular reaction both thermodynamically and kinetically, because the reaction would induce less strain and would have an increased attempt frequency.

This work represents an advance over previous attempts to control assembly order. One previous approach imposes assembly order by designing different parts of the structure to have distinct melting or formation temperatures, usually by using binding domains of different lengths. The assembly events thus occur in a particular order as the temperature is lowered during the annealing process. This has been used a number of times,[38,39] including with some polyhedra.[40,41] However, such approaches typically require external modulation of the assembly environment in the form of an annealing ramp, coupling the assembly order to bulk environmental conditions such as temperature. Also, while other approaches have recently been demonstrated that work isothermally within narrow ranges of temperatures,[20] no explicit assembly order control is designed in these systems. In contrast, our approach allows direct, molecular-level control of assembly order through complete pathway engineering, is independent of bulk properties like temperature, and operates isothermally over a wide range of temperatures that includes biologically relevant conditions.

Another route for direct isothermal molecular control of assembly order is the algorithmic self-assembly of static DNA tiles .[4,10,42] Here, in a seeded growth system,

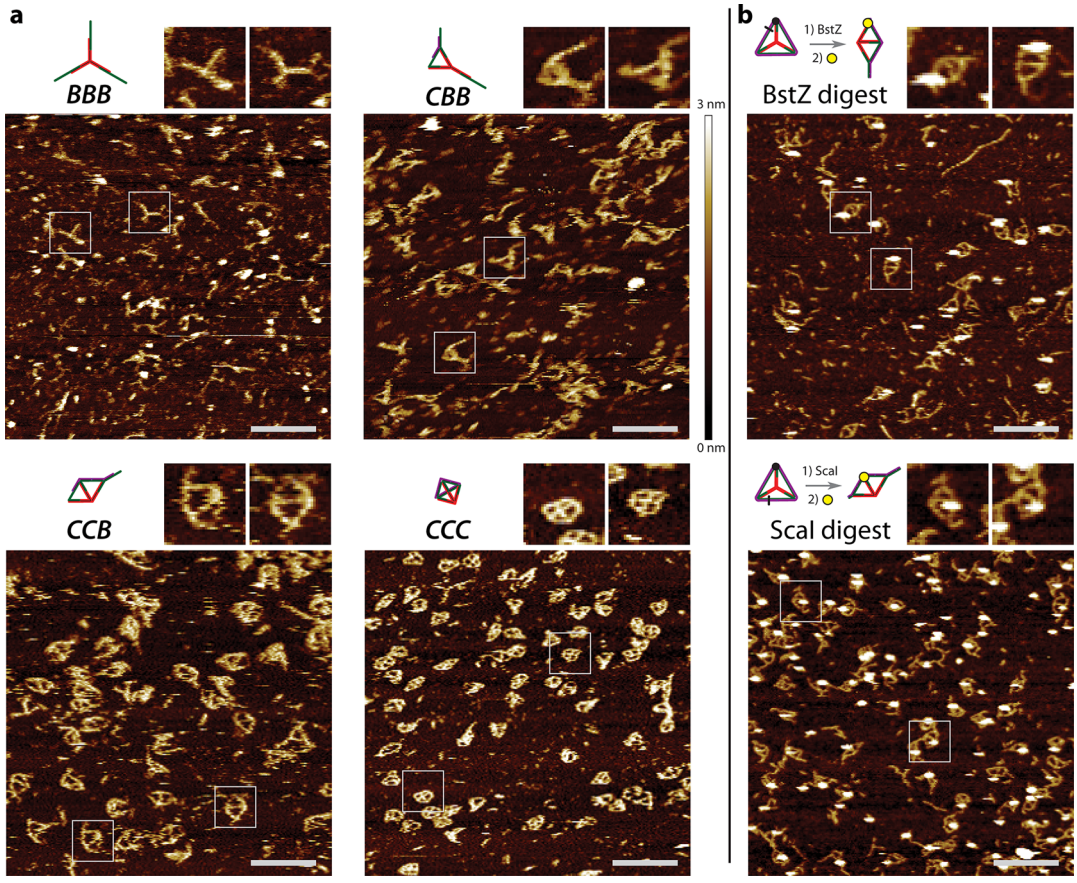

Figure 4. Atomic force microscopy images of tetrahedron self-assembly. (a) Images of purified samples of the intermediates *BBB*, *CBB*, *CCB*, and the full tetrahedron *CCC*, which, respectively, appeared as a three-arm junction, a single triangle, a double triangle, and a three- or four-lobed structure corresponding to a flattened tetrahedron, each consistent with our design. In each image, the double-stranded edges of each wireframe structure are clearly resolved. (b) Images of the full tetrahedron cut by restriction endonucleases followed by incubation with streptavidin. Digestion with either of two endonucleases targeted to different edges restored the double-triangle structures, with the streptavidin (appearing as small white circular features in the AFM image) appearing at the expected biotin-modified vertices. In the schematic diagrams, the black bar intersecting tetrahedron edge represents the designed restriction site, the black dot is the 5′-biotin, and the yellow circle is the streptavidin. The scale bars of the larger images are 100 nm long; the inset images are 62.5 nm in width, at double the scale of the larger images. These samples were assembled at a concentration of 100 nM and then purified by glycerol gradient ultracentrifugation; for panel b, the restriction and streptavidin binding were performed before purification.

tiles are incorporated sequentially at particular positions, as directed by cooperative binding to neighboring tiles on the growth front. However, this tile-based approach is dependent upon the supersaturated nature of the tile species, and is limited to the specific geometry of tile-based lattices with a growth front. More broadly, this tile-based approach involves "static" monomers incorporated by simple binding to the growing structure without explicitly designed internal state changes. In contrast to "passive" assembly using static tiles, our "active" developmental self-assembly uses reconfigurable hairpins as assembling monomers that are capable of conditional configurational change and can implement both assembly and disassembly. An analytical model has found that methods using active components can in principle be exponentially faster than the corresponding passive methods.[43] Developmental assembly with active components provides a more versatile, expressive molecular programming language for integrating temporal and spatial control, and a potentially more efficient method for the active construction of molecular structures.

Kinetically controlled developmental self-assembly mimics the well-orchestrated nature of biological reaction cascades, which operate autonomously and without the need for external intervention to maintain their function. The triggered, isothermal nature of our assembly methodology would allow the formation of complex structures to be integrated with nucleic acid computational circuits, allowing the use of structural changes as an output mode of logical computation. These could furthermore be interfaced with non-nucleic acid inputs such as proteins and small molecules through the use of aptamers,[30] which would allow these systems to interact with the larger chemical world and respond in potentially intricate ways to their molecular environment. This methodology is additionally expected to be more amenable to *in vivo*

applications, where thermal annealing is not an available mode of assembly. Thus, synthetic developmental self-assembly promises to open new doors to bridge computation, chemistry, and biology.

EXPERIMENTAL METHODS

Sequence Design. Motif design was performed by hand using principles described previously[28] and in Supporting Information Section S3.1. Sequence design was performed with Multisubjective (version 1.0.2), a program that identifies and eliminates spurious hybridizations in the full hairpin system (manuscript in preparation), in association with Domain Design (DD) (version 0.2), which uses simple heuristics to evaluate the acceptability of candidate sequence domains.[44] A local copy of NUPACK (version 3.0) was used by Multisubjective to generate base-pairing probabilities for further analysis.[45,46] See Supporting Information Section S3.2 for more sequence design details. See Supporting Information Section S5 for designed sequences.

Strand Synthesis. DNA strands were synthesized and purified by Integrated DNA Technologies (IDT), including strands containing phosphates and fluorophores. For the fluorescent **C** strands used in the fluorescence-quenching assay only, we ordered the strands in two halves, ligated them using 27 U/μL of T4 DNA ligase at a DNA concentration of 27 μM at 16 °C for 2 h, and purified the product by denaturing polyacrylamide gel electrophoresis. In all cases, we quantitated the concentrations of DNA stock solutions by measuring the ultraviolet light absorption at 260 nm with the microvolume pedestal of a NanoDrop 2000c spectrophotometer, taking the average of measurements of three samples for each strand, and using extinction coefficients provided by IDT to calculate the concentration of each strand.

Sample Preparation. The hairpin strands were separately heated to 95 °C for 5 min and allowed to cool to room temperature over about 20 min. Cooperative hybridization complexes were annealed in the same way, except that 1.5 equiv of the **Cp** strands was combined with 1 equiv of the **C** strand before annealing. The desired reactants were then combined to a final concentration of 100 nM (Figure 2, lanes 1−30 and Figure 4) or 10 nM (Figure 2, lanes 31−35 and Figure 3) of each reactant except **A1**, for which 0.9 equiv was used instead in order to obviate the effects of inaccuracies in stoichiometry and assist in calculation of the yield. The assembly reactions were performed at room temperature over about 20 h in TAE/Mg^{2+} buffer containing 40 mM Tris base, 20 mM acetic acid, 12.7 mM EDTA, and 12.5 mM $MgCl_2$.

For the formation assay (Figure 2), an **A1** strand incorporating a fluorescent label was used instead of the regular **A1** strand. For the fluorescence-quenching assay (Figure 3), the **C** strands each had a different fluorophore on one end and an optional quencher on the other, as described in the figure caption. For the ***CCC*** samples in the atomic force microscopy studies (Figure 4a), we used **C** strands that contained phosphates on their 5′-ends; this was not expected to affect the assembly. For the streptavidin labeling experiment (Figure 4b), we used an **A2** strand containing a 5′ biotin.

For the atomic force microscope studies, the samples were purified by ultracentrifugation in a 15−45% glycerol gradient in 1× TAE/Mg^{2+} for 3 h at 50 000 rpm. Fractions of 100 μL were taken from the centrifuge tube, and the fractions containing the desired product were identified by native gel electrophoresis. The glycerol was not removed after the purifications, meaning that subsequent manipulations were performed in buffer containing about 20% glycerol.

Gel Electrophoresis. The gels in Figures 2 and 3 were precast 6% native polyacrylamide gels run at 100 V for 55 min at 21 °C using 1× TBE running buffer. For each lane, 4 μL of the reaction mixture was mixed with an equal amount of 2× native loading buffer containing a small amount of bromophenol blue in 2× TAE/Mg^{2+} buffer and 10% glycerol. Then, 4 μL of this mixture containing 0.2 pmol of the specified complex was then loaded into the gel.

The gels were imaged with a Typhoon FLA 9000 gel scanner. The gels in Figure 2 and the right side inset of Figure 3 were stained in SYBR Gold for about 20 min before imaging; all other gels were unstained. For Figure 2, we imaged the gel unstained using the fluorescent label, and then stained it and reimaged the same gel. The two images were then manually overlaid.

We quantitated the yield by dividing the fluorescence intensity of the desired product by the intensity of the entire lane in the fluorescently labeled channel (shown as red) in Figure 2, using ImageQuant TL. We used automatic band detection for the bands representing the desired product, and the reactants band if it was present. We then defined multimers as the lane area with lower mobility than the desired product band, and intermediates as the lane area between the product and reactants band. For background subtraction, we used the rolling ball method with a radius of 500.

Atomic Force Microscopy. The samples in Figure 4a were imaged directly after glycerol purification. For the streptavidin labeling experiment (Figure 4b), the appropriate digestion buffer was added after assembly to a final concentration of 1×, and the structures were digested with one of the two restriction endonucleases BstZ17I or ScaI-HF at a concentration of 1 U/μL at 37 °C for 2 h. The structures were then incubated with a 10× solution of streptavidin for 30 min and then glycerol purified.

For imaging, we added to a freshly cleaved mica surface, 30 μL of filtered 5× TAE/Mg^{2+} buffer, followed by 30 μL of a 10 mM solution of $NiCl_2$ to increase the strength of the DNA−mica binding. After 5 min, we added 10−30 μL of the glycerol-purification fraction containing our desired product. AFM images were obtained using a Multimode 8 scanning probe microscope with a Digital Instruments Nanoscope V controller. Images were collected in aqueous phase using tapping mode, using the short and thin cantilevers in the SNL-10 silicon nitride cantilever chip. Within each of the two panels of Figure 4, the images were all generated using the same tip.

Conflict of Interest: The authors declare no competing financial interest.

Acknowledgment. The authors thank C. Grun and E. Winfree for discussions, and D. Pastuszak for help with draft preparation. This work was funded by Office of Naval Research Grants N000141010827 and N000141310593, Office of Naval Research Young Investigator Program Award N000141110914, NIH Director's New Innovator Award 1DP2OD007292, NSF CAREER Award CCF1054898, NSF Grant CCF1162459, NSF Expedition in Computing Award CCF1317291, and Wyss Institute for Biologically Inspired Engineering Faculty Startup Fund to P.Y., and NIH 5R01CA140759, NIH P50 HG004071, the Molecular Programming Project (NSF-CCF-0832824 and NSF-CCF-1317694), and the Gordon and Betty Moore Foundation (GBMF2809) to N.A.P.; J.P.S. acknowledges a Graduate Research Fellowship from NSF and a J. Marshall & Jane H. Booker Graduate Scholarship from the Buttonwood Foundation, and D.Y.Z. is supported by NIH Transition to Independence Award 1K99EB015331.

Supporting Information Available: Expanded versions of figures, additional experimental characterization of the tetrahedron assembly, discussion of design considerations, experimental characterization of alternate tetrahedron structures, discussion of the nodal reaction graph abstraction, and strand sequences. This material is available free of charge *via* the Internet at http://pubs.acs.org.

REFERENCES AND NOTES

1. Seeman, N. C. Nucleic Acid Junctions and Lattices. *J. Theor. Biol.* **1982**, *99*, 237–247.
2. Seeman, N. C. DNA in a Material World. *Nature* **2003**, *421*, 427–431.

3. Shih, W. M.; Lin, C. Knitting Complex Weaves with DNA Origami. *Curr. Opin. Struct. Biol.* **2010**, *20*, 276–282.
4. Schulman, R.; Winfree, E. Synthesis of Crystals with a Programmable Kinetic Barrier to Nucleation. *Proc. Natl. Acad. Sci. U.S.A.* **2007**, *104*, 15236–15241.
5. Yin, P.; Hariadi, R.; Sahu, S.; Choi, H. M. T.; Park, S. H.; LaBean, T. H.; Reif, J. H. Programming Molecular Tube Circumferences. *Science* **2008**, *321*, 824–826.
6. Yan, H.; Park, S. H.; Finkelstein, G.; Reif, J. H.; LaBean, T. H. DNA-Templated Self-Assembly of Protein Arrays and Highly Conductive Nanowires. *Science* **2003**, *301*, 1882–1884.
7. Winfree, E.; Liu, F.; Wenzler, L. A.; Seeman, N. C. Design and Self-Assembly of Two-Dimensional DNA Crystals. *Nature* **1998**, *394*, 539–544.
8. Yan, H.; LaBean, T. H.; Feng, L.; Reif, J. H. Directed Nucleation Assembly of DNA Tile Complexes for Barcode-Patterned Lattices. *Proc. Natl. Acad. Sci. U.S.A.* **2003**, *100*, 8103–8108.
9. Liu, D.; Wang, M.; Deng, Z.; Walulu, R.; Mao, C. Tensegrity: Construction of Rigid DNA Triangles with Flexible Four-Arm DNA Junctions. *J. Am. Chem. Soc.* **2004**, *126*, 2324–2325.
10. Rothemund, P. W. K.; Papadakis, N.; Winfree, E. Algorithmic Self-Assembly of DNA Sierpinski Triangles. *PLoS Biol.* **2004**, *2*, 2041–2053.
11. Zheng, J. P.; Birktoft, J.; Chen, Y.; Wang, T.; Sha, R. J.; Constantinou, P.; Ginell, S.; Mao, C. D.; Seeman, N. C. From Molecular to Macroscopic *via* the Rational Design of a Self-Assembled 3D DNA Crystal. *Nature* **2009**, *461*, 74–77.
12. Chen, J.; Seeman, N. C. The Synthesis from DNA of a Molecule with the Connectivity of a Cube. *Nature* **1991**, *350*, 631–633.
13. Rothemund, P. W. K. Folding DNA to Create Nanoscale Shapes and Patterns. *Nature* **2006**, *440*, 297–302.
14. He, Y.; Ye, T.; Su, M.; Zhang, C.; Ribbe, A. E.; Jiang, W.; Mao, C. Hierarchical Self-Assembly of DNA into Symmetric Supramolecular Polyhedra. *Nature* **2008**, *452*, 198–201.
15. Douglas, S. M.; Dietz, H.; Liedl, T.; Högberg, B.; Graf, F.; Shih, W. M. Self-Assembly of DNA into Nanoscale Three-Dimensional Shapes. *Nature* **2009**, *459*, 414–418.
16. Dietz, H.; Douglas, S. M.; Shih, W. M. Folding DNA into Twisted and Curved Nanoscale Shapes. *Science* **2009**, *325*, 725–730.
17. Han, D.; Pal, S.; Nangreave, J.; Deng, Z.; Liu, Y.; Yan, H. DNA Origami with Complex Curvatures in Three-Dimensional Space. *Science* **2011**, *332*, 342–346.
18. Wei, B.; Dai, M.; Yin, P. Complex Shapes Self-Assembled from Single-Stranded DNA Tiles. *Nature* **2012**, *485*, 623–626.
19. Ke, Y.; Ong, L.; Shih, W.; Yin, P. Three-Dimensional Structures Self-Assembled from DNA Bricks. *Science* **2012**, *338*, 1177–1183.
20. Sobczak, J.; Martin, T.; Gerling, T.; Dietz, H. Rapid Folding of DNA into Nanoscale Shapes at Constant Temperature. *Science* **2012**, *338*, 1458–1461.
21. Han, D.; Pal, S.; Yang, Y.; Jiang, S.; Nangreave, J.; Liu, Y.; Yan, H. DNA Gridiron Nanostructures Based on Four-Arm Junctions. *Science* **2013**, *339*, 1412–1415.
22. Zhang, D. Y.; Seelig, G. Dynamic DNA Nanotechnology Using Strand-Displacement Reactions. *Nature Chem.* **2011**, *3*, 103–113.
23. Bath, J.; Turberfield, A. J. DNA Nanomachines. *Nat. Nanotechnol.* **2007**, *2*, 275–284.
24. Yurke, B.; Turberfield, A. J.; Mills, A. P.; Simmel, F. C.; Neumann, J. L. A DNA-Fuelled Molecular Machine Made of DNA. *Nature* **2000**, *406*, 605–608.
25. Yan, H.; Zhang, Z.; Shen, X.; Seeman, N. C. A Robust DNA Mechanical Device Controlled by Hybridization Topology. *Nature* **2002**, *415*, 62–65.
26. Seelig, G.; Soloveichik, D.; Zhang, D. Y.; Winfree, E. Enzyme-Free Nucleic Acid Logic Circuits. *Science* **2006**, *314*, 1585–1588.
27. Zhang, D.; Turberfield, A.; Yurke, B.; Winfree, E. Engineering Entropy-Driven Reactions and Networks Catalyzed by DNA. *Science* **2007**, *318*, 1121–1125.
28. Yin, P.; Choi, H. M. T.; Calvert, C. R.; Pierce, N. A. Programming Biomolecular Self-Assembly Pathways. *Nature* **2008**, *451*, 318–322.
29. Qian, L.; Winfree, E. Scaling Up Digital Circuit Computation with DNA Strand Displacement Cascades. *Science* **2011**, *332*, 1196–1201.
30. Dirks, R.; Pierce, N. Triggered Amplification by Hybridization Chain Reaction. *Proc. Natl. Acad. Sci. U.S.A.* **2004**, *101*, 15275–15278.
31. Venkataraman, S.; Dirks, R.; Rothemund, P.; Winfree, E.; Pierce, N. An Autonomous Polymerization Motor Powered by DNA Hybridization. *Nat. Nanotechnol.* **2007**, *2*, 490–494.
32. Sherman, W. B.; Seeman, N. C. A Precisely Controlled DNA Biped Walking Device. *Nano Lett.* **2004**, *4*, 1203–1207.
33. Shin, J.-S.; Pierce, N. A Synthetic DNA Walker for Molecular Transport. *J. Am. Chem. Soc.* **2004**, *126*, 10834–10835.
34. Yin, P.; Yan, H.; Daniell, X.; Turberfield, A. J.; Reif, J. A Unidirectional DNA Walker That Moves Autonomously along a Track. *Angew. Chem. Int. Ed.* **2004**, *43*, 4906–4911.
35. Omabegho, T.; Sha, R.; Seeman, N. C. A Bipedal DNA Brownian Motor with Coordinated Legs. *Science* **2009**, *324*, 67–71.
36. Nanorex, Inc. Nanoengineer-1. http://nanoengineer-1.com/ The original website is no longer available as of this writing; an archived version is available at http://web.archive.org/web/20121218/http://www.nanoengineer-1.com/content/, accessed April 8, 2014.
37. Zhang, D. Y. Cooperative Hybridization of Oligonucleotides. *J. Am. Chem. Soc.* **2011**, *133*, 1077–1086.
38. Kumara, M. T.; Nykypanchuk, D.; Sherman, W. B. Assembly Pathway Analysis of DNA Nanostructures and the Construction of Parallel Motifs. *Nano Lett.* **2008**, *8*, 1971–1977.
39. Snyder, T. M.; Liu, D. R. Ordered Multistep Synthesis in a Single Solution Directed by DNA Templates. *Angew. Chem. Int. Ed.* **2005**, *44*, 7379–7382.
40. Shih, W.; Quispe, J.; Joyce, G. A 1.7-Kilobase Single-Stranded DNA That Folds into a Nanoscale Octahedron. *Nature* **2004**, *427*, 618–621.
41. Goodman, R.; Schaap, I.; Tardin, C.; Erben, C.; Berry, R.; Schmidt, C.; Turberfield, A. Rapid Chiral Assembly of Rigid DNA Building Blocks for Molecular Nanofabrication. *Science* **2005**, *310*, 1661–1665.
42. Barish, R. D.; Schulman, R.; Rothemund, P. W. K.; Winfree, E. An Information-Bearing Seed for Nucleating Algorithmic Self-Assembly. *Proc. Natl. Acad. Sci. U.S.A.* **2009**, *106*, 6054–6059.
43. Woods, D.; Chen, H.-L.; Goodfriend, S.; Dabby, N.; Winfree, E.; Yin, P. Active Self-Assembly of Algorithmic Shapes and Patterns in Polylogarithmic Time. In *ITCS 2013: Innovations in Theoretical Computer Science*; Association for Computing Machinery: Berkeley, CA, 2013; pp 353−354.
44. Zhang, D. Y. Towards Domain-Based Sequence Design for DNA Strand Displacement Reactions. *Lect. Notes Comput. Sci.* **2011**, *6518*, 162–175.
45. Dirks, R. M.; Bois, J. S.; Schaeffer, J. M.; Winfree, E.; Pierce, N. A. Thermodynamic Analysis of Interacting Nucleic Acid Strands. *SIAM Rev.* **2007**, *49*, 65–88.
46. Zadeh, J. N.; Steenberg, C. D.; Bois, J. S.; Wolfe, B. R.; Pierce, M. B.; Khan, A. R.; Dirks, R. M.; Pierce, N. A. NUPACK: Analysis and Design of Nucleic Acid Systems. *J. Comput. Chem.* **2011**, *32*, 170–173.